

Mitigating KV Cache Competition to Enhance User Experience in LLM Inference

Haiying Shen
University of Virginia

Tanmoy Sen
University of Virginia

Masahiro Tanaka
Microsoft

Abstract

In Large Language Model (LLM) serving, the KV-cache (KVC) bottleneck causes high tail Time-to-First-Token (TTFT) and Time-Between-Tokens (TBT), impairing user experience, particularly in time-sensitive applications. However, satisfying both TTFT and TBT service-level objectives (SLOs) is challenging. To address this, we propose a system, named CACHEOPT for mitigating KV Cache competition, based on key insights from our measurements, incorporating novel components. First, it estimates a request’s output length, bounding the deviation with a high specified probability, adjusted based on the request arrival rate. Second, it allocates the estimated KVC demand to a request, and reuses other requests’ allocated KVC to avoid preemptions while reducing waiting time. Third, it proactively allocates KVC before instead of at the time a request exhausts its allocation and reserves KVC globally to prevent preemptions. Fourth, it chooses a request that has long TBT SLO, long job remaining time and short preemption time to preempt. Fifth, it selects the shortest-latency strategy between swapping and recomputation for preemptions. Experiments show that CACHEOPT achieves up to $3.29\times$ and $2.83\times$ lower tail TBT and tail TTFT, 47% and 53% higher TTFT and TBT SLO attainments, and supports up to $1.58\times$ higher request arrival rate than the state-of-the-art methods.

1 Introduction

The Large Language Model (LLM) models have found widespread applications across various domains, including automated customer support, chatting, and real-time translation. However, deploying LLMs in real-world applications often comes with high tail Time-to-First-Token (TTFT) or Time-Between-Tokens (TBT) [1–3], which can impair user experience, especially in time-sensitive tasks. Reducing TTFT and TBT is crucial for ensuring seamless user interactions and satisfied user experience. It also enables the broader adoption of LLMs in different applications.

Due to limited GPU memory and the large volume of KV-cache (KVC) values, KVC becomes a bottleneck, significantly impacting both TTFT and TBT. The first iteration-level scheduler ORCA [4] pre-allocates KVC for the maximum sequence length for each request. However, this approach wastes memory [5], limits the batch size and hence GPU utilization (e.g., 0.4% [5]) and throughput. To address this problem, vLLM [6] uses block-based KVC allocation approach, in which, a block, consisting of a fixed number of tokens, is allocated to a request each time. To form a batch in each iteration, the requests from the waiting queue are added to the batch until the whole KVC is allocated. While this approach significantly reduces KVC reserved waste, a running request may experience block allocation failure when it exhausts its allocation. In this case, the last arrived running request is selected to preempt based on the first-in-first-serve (FCFS) policy. Both approaches introduce delays, increasing TBT.

Another method allocates KVC to a request equal to the response length predicted by an LLM model [7, 8]. Compared to the block-based allocation approach, it reduces the chances of KVC allocation failures but still leads to certain reserved waste since allocated KVC is not used instantly and generates KVC allocation failures with underestimation. [7] proposes to add a constant padding (e.g., 100 tokens) to the predicted value to avoid underprovisioning, indicates that overprovision is not as important as underprovision.

Different LLM applications and users often have varying SLOs for TTFT and TBT. For example, real-time translation applications prioritize ultra-low TTFT to deliver the first token as quickly as possible, enabling smoother conversation flow. In contrast, document summarization may tolerate higher TTFT in exchange for lower TBT. Moreover, users’ reading speeds influence their tolerance for TBT. A fast reader using a summarization tool may prefer shorter TBT to maintain a seamless reading experience, while a slower reader may be less sensitive to longer TBT but require low TTFT for responsiveness. The diverse demands necessitate adaptable LLM systems capable of meeting varying TTFT and TBT SLOs.

In this paper, we aim to mitigate KV cache competition

while enhancing user experience by satisfying the diverse TTFT and TBT SLOs through studying three problems:

- (1) How to determine the padding size to ensure that the KVC demand is satisfied with a high specified probability?
- (2) How to allocate KVC to a request initially and during token generation process?
- (3) How to choose requests to preempt?
- (4) How to choose a preemption strategy between swapping and recomputation to reduce the preemption time (defined as the time that a request is halted)?

To achieve this goal, we conducted an experiments based on real traces and made the following observations (Os):

- (1) Block-based KVC allocation increases preemptions and TBT, while prediction-based allocation raises TTFT. A new method is needed to balance both.
- (2) Previous prediction-based methods often cause underprovisioning (increasing TBT) and overprovisioning (increasing TTFT). The padding size must be carefully determined, considering the request arrival rate, to balance TTFT and TBT.
- (3) FCFS-based preemption results in more preemptions than approaches that account for remaining time and KVC usage.
- (4) For sequences exceeding the sweet spot length, swapping results in shorter times compared to recomputation.

Leveraging these observations, we propose a system, that optimizes the cache operations for mitigating KV cache competition (CACHEOPT). We name this CACHEOPT to reflect the system’s focus on efficient cache usage. CACHEOPT consists of the following components.

- (1) **Confidence-based Padding.** We modify an LLM model to predict output length and deviation direction for adding or subtracting padding. Using Hoeffding’s inequality theory [9, 10], we determine the padding needed to ensure a request’s KVC demand is satisfied with a high specified probability and adjust it based on arrival rate to balance TTFT and TBT. (O2)
- (2) **SLO-aware Batching and KVC Allocation.** We reuse allocated but unused KVC and select waiting and returned requests that must run to satisfy their TTFT and TBT SLOs. The remaining unallocated KVC is distributed among the selected requests to maximize throughput. Additionally, it proactively allocates KVC before instead of at the time a request exhausts its allocation and reserves KVC globally to prevent preemptions. (O1)
- (3) **Preemption Policy.** We order requests for preemption based on their latency SLO, remaining completion time and KVC occupancy in order to avoid SLO violation and preemptions, and reduce preemption time. (O3)
- (4) **Preemption Strategy Selection.** When the KVC size exceeds the observed sweet spot sequence length, we opt for swapping; otherwise, we choose recomputation. (O4)

Experimental results show that CACHEOPT achieves up to a $3.29\times$ and $2.83\times$ lower tail TBT and TTFT and 47% and 53% higher TTFT and TBT SLO attainments than the state-of-the-art methods, respectively. We will distribute CACHEOPT’s source code after the paper is accepted.

Table 1: Trace properties and experiment settings.

Trace	Input length			Output length			Number of requests	Mean arrival rate
	avg	min	max	avg	min	max		
Alpaca	19.31	9	2.47K	58.41	13	292	52K	32
ShareGPT	161.31	16	3.2K	337.99	19	991	90K	28
BookCorpus	1952.11	18	461K	681.2	32	1041	11K	1.2

2 Experimental Analysis

2.1 Experiment Settings

Machine settings. We used an AWS p4d.24xlarge instance, which features 8 NVIDIA A100 GPUs. Each GPU has 80GB of memory. The GPUs are interconnected via a 600 GB/s NVSwitch. We executed the OPT-13B model [11] on a single GPU, and the OPT-175B model, partitioning the model across 8 GPUs with both model and tensor parallelism degree of 2 as in [4].

Request settings. We used the Alpaca [12], ShareGPT [13], and BookCorpus [14] traces. Table 1 shows their features and the mean request arrival rate setting. It follows a Poisson distribution [4, 6]. The block size was set to 32. For BookCorpus [14], we divided the prompts into 2048 tokens to meet the requirements of the LLM models. We used 3-hour trace for OPT-13B and 1-hour trace for OPT-175B.

Schedulers. We conducted the experiment measurements for the following methods. 1) Response Length Prediction (RLP) [7] uses the LLM to predict the response length from a request and always adds a padding of 100 tokens. It tries to schedule the requests with similar lengths in the same batch. Any underprovisioned requests are preempted and later executed when there is sufficient KVC. 2) S^3 [8] uses the LLM model to predict the response length bucket (with a 50-token increment) for each request and allocates the upper bound of the predicted bucket. If a request faces insufficiently allocated KVC, it is preempted, and its KVC demand is doubled for the next allocation. 3) vLLM [6] uses the block-based KVC allocation and FCFS-based preemption, and defers new requests until preempted ones are completed.

To make these methods comparable, we used our own fine-tuned OPT-13B model for the response length prediction in RLP and S^3 . To avoid the interference on the LLM inference, we ran this model in another server. In this paper, *predicted output length* refers to the output length from the LLM, and *estimated output length* refers to the predicted output length adjusted with the padding.

2.2 Impact of KVC Allocation Methods on TTFT and TBT

Although [7] indicates that overprovisioning is less critical than underprovisioning, this claim primarily applies to requests with overprovisioning. However, overprovisioning reduces the number of requests accommodated in a batch, increasing waiting time and TTFT. A request’s *waiting time*

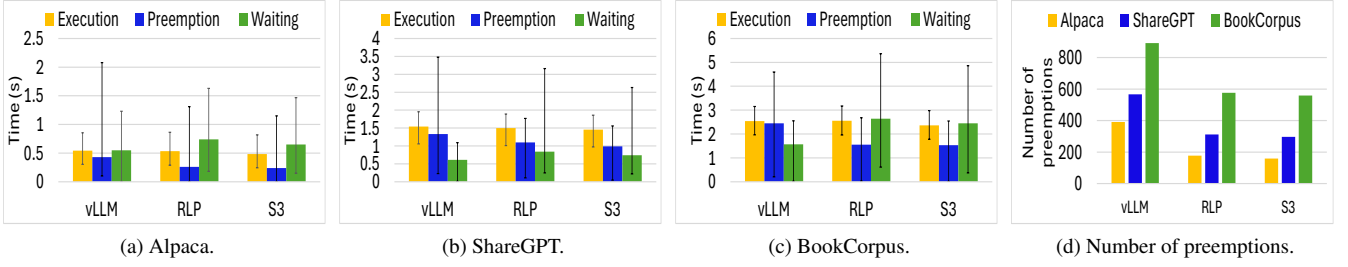


Figure 1: Measurements for different traces for OPT-13B.

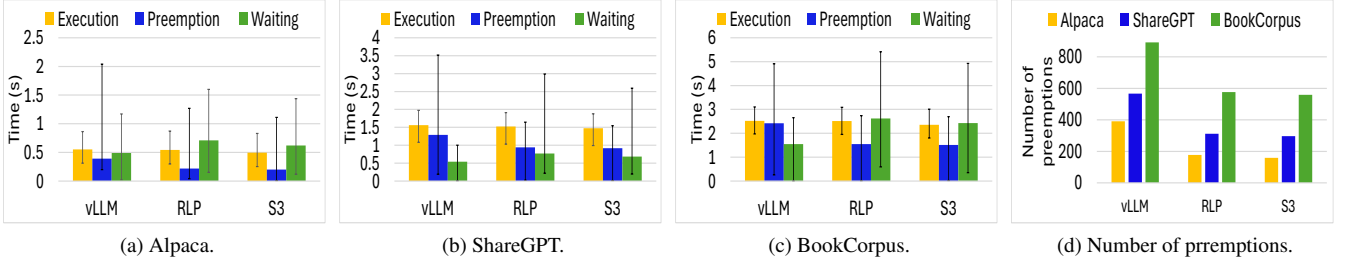


Figure 2: Measurements for different traces for OPT-175B.

is the duration its prompt remains in the queue before execution begins; and its *execution time* is the duration from when it is dispatched to the execution engine until completion, excluding preemption time. Figures 1a-1c and Figure 2a-2c show the average execution, preemption, and waiting times for OPT-13B and OPT-175B, with error bars representing the min and max values. RLP and S^3 generate 29%-49% and 26%-45% lower preemption time but 43%-72% and 27%-65% higher waiting time than vLLM. This is because that in vLLM, each request is only allocated with a block at a time, and it has to be preempted upon KVC allocation failure when it uses up its allocated block. RLP and S^3 allocate to a request the KVC equal to its estimated sequence length, so they reduce the number of requests accommodated in a batch and increase the TTFT but reduce the preemption time, which occurs only at underprovisioning. These findings are verified in Figure 2d, which shows the average number of preemptions, and Figure 3, which shows the average number of requests added to the batch per iteration, with error bars representing the minimum and maximum values. S^3 has 7% lower preemption time, 5% lower waiting time, and adds 12-17% more requests to the batch per iteration than RLP since S^3 adds 100-token padding while RLP's bucket size is 50. We calculated that the preemption time and the waiting time can take up to 71% and 75% of the execution time on average across the three datasets.

We find the *token budget* for the number of tokens in a batch to maximize throughput as in [15]. Figure 4 shows the average token budget used and the average number of allocated KVC tokens at each iteration. We see that while all systems fully allocate the KVC, vLLM more fully utilizes the token budget than RLP and S^3 by 37% and 33%.

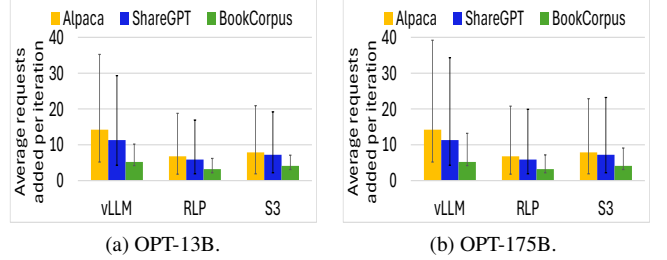


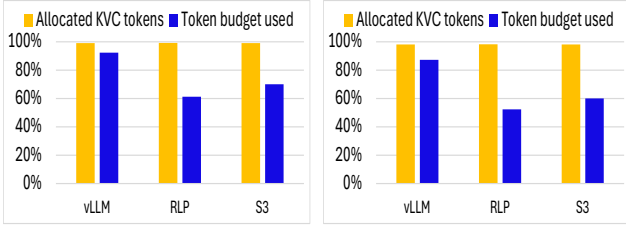
Figure 3: Average requests added per iteration.

Observation 1. Due to KVC bottleneck, the block-based KVC allocation method increases preemptions and TBT, while the prediction-based KVC allocation method increases request waiting time and TTFT. A novel approach is required to limit both TTFT and TBT effectively.

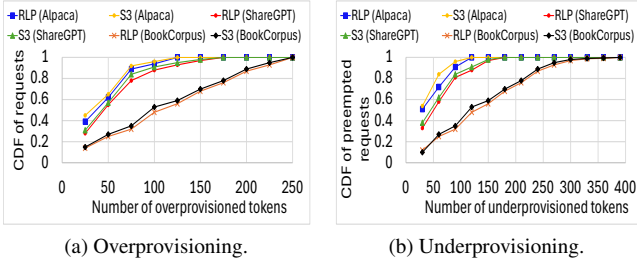
2.3 Padding Size Determination and Impact

Figures 5 shows the CDF of requests versus the number of over and under provisioned tokens for RLP and S^3 . Overprovisioning and underprovisioning are consistently observed. Different requests exhibit varying degrees of these deviations, with longer prompts generally experiencing greater overprovisioning and underprovisioning amounts.

Figure 6 shows the response latency decomposed to waiting time, preemption time and execution time versus different padding size at different arrival rate for RLP. At each arrival rate, we observe that as the padding size increases, the pre-



(a) OPT-13B. (b) OPT-175B.
Figure 4: Illustration of resource bottleneck.



(a) Overprovisioning. (b) Underprovisioning.
Figure 5: CDF of requests vs. over/under provisioned tokens.

emption time decreases, the waiting time increases, and the execution time remains stable. The total response latency exhibits a concave pattern, initially decreasing with smaller padding sizes and then increasing beyond a certain threshold. Also, the arrival rate increase leads to higher waiting time. The padding size that minimizes the response latency varies for different arrival rates.

Observation 2. Previous prediction-based methods often cause underprovisioning (increasing TBT) and overprovisioning (increasing TTFT). The padding size must be carefully determined, considering the request arrival rate, to balance TTFT and TBT.

2.4 Preemption Policy

In RLP, we used the following preemption policies that preempt the request: 1) with the latest arrival time based on FCFS employed in vLLM, 2) with the longest remaining time based on the Shortest-Remaining-Time-First (SRTF), and 3) with the smallest occupied KVC based on the Lowest-KVC-occupancy (LKVO). Figure 7 shows the tail preemption time and total number of preemptions, respectively. FCFS exhibits 26%-58% and 39%-1.03 \times higher tail preemption time, 9%-31% and 13%-39% more preemptions compared to LKVO and SRTF, respectively. SRTF helps reduce KVC competition by making running requests release their KVC sooner, thus lowering preemptions. LKVO minimizes the time spent on swapping or recomputation.

Observation 3. FCFS leads to more frequent preemptions and increased preemption time compared to SRTF and LKVO.

2.5 Preemption Strategy: Swapping or Recomputation?

The time complexity of swapping is $O(s)$ and that of recomputation is $O(s^2)$, where s is the sequence length. Figure 8 shows the latency for swapping including swapping in and out and recomputation for the varying sequence length. It confirms that swapping follows a linear growth, while recomputation follows a quadratic growth based on the sequence length. We observe that swapping is faster when the sequence length exceeds 4000 tokens; otherwise, recomputation is faster. However, vLLM and RLP use recomputation and S³ uses swapping as the default preemption strategy irrespective of the sequence length, and users can choose a strategy at a time.

Observation 4. Relying on a single preemption strategy is inefficient. When the sequence length exceeds a threshold (e.g., 4k in our setting), swapping is faster than recomputation.

3 System Design

3.1 Solution Overview

Based on our observations, we propose CACHEOPT. CACHEOPT consists of the following components as shown in Figure 9.

- (1) *Confidence-based padding* guided by O2 (3.2).
- (2) *SLO-aware batching and KVC allocation* per O1 (3.3).
- (3) *Preemption policy* guided by O3 (3.4).
- (4) *Preemption strategy selection* guided by O4 (3.5).

In Figure 9, users' requests are initially entered to the waiting queue. *Confidence-based padding* (①) is executed to estimate the output length of each request when it waits in the queue. After each iteration, *SLO-aware batching and KVC allocation* (②) selects waiting requests to form a batch and allocates KVC to each batched request. Next, the batch is forwarded to the execution engine to be executed. When a request experiences under-provisioning, the *preemption policy* (③) is executed to choose the requests to be preempted. The preempted requests are entered to the waiting queue and ordered. For a request to be preempted, the *preemption strategy selection* (④) is executed to reduce the preemption time of this request and other running requests.

3.2 Confidence-based Padding

Given the autoregressive nature of LLMs, accurately predicting the response length of a request poses a challenge. RLP achieves an accuracy of 67% [7], while S³ reaches 79% [8], resulting in overprovisioning and underprovisioning and increasing TTFT and TBT (O2). To address this issue, we pro-

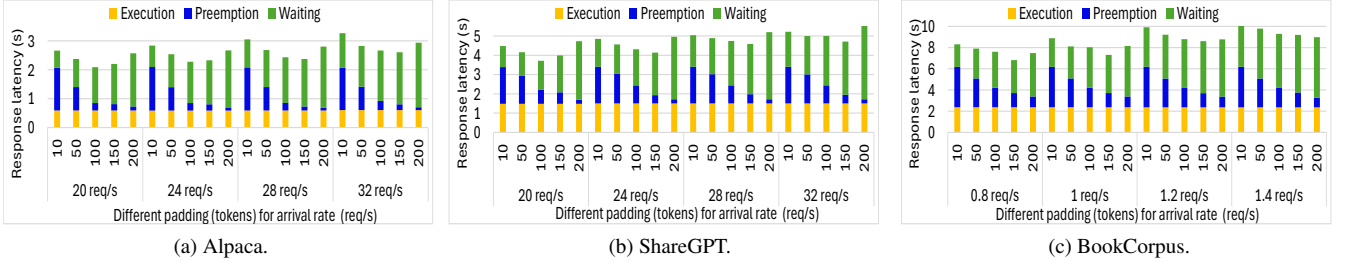


Figure 6: Trade-off between preemption time and waiting time versus padding size for OPT-13B.

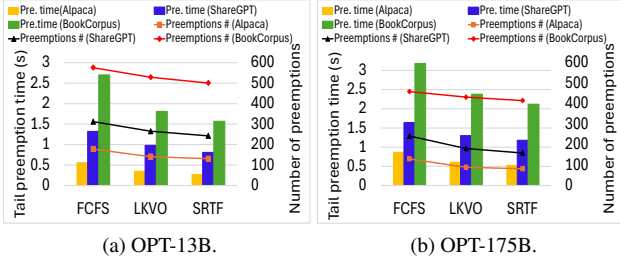


Figure 7: Performance of different preemption policies

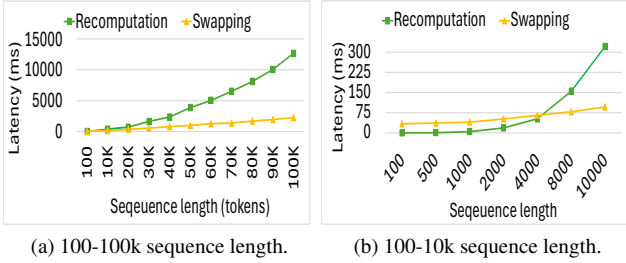


Figure 8: Latency of swapping and recomputation.

pose a confidence-based padding method, leveraging Hoeffding’s inequality to bound overprovisioning and underprovisioning with high probability or confidence.

Output length prediction. Previous methods relying on LLMs to predict output length lack the ability to provide high confidence to bound the overprediction or underprediction, or to identify the deviation direction. Our method addresses these issues. As in [7], we use OPT-13B as the base model

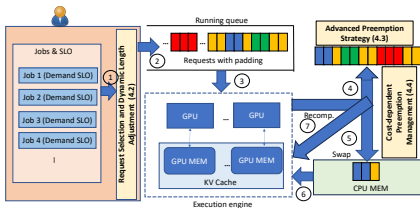


Figure 9: Architecture of CACHEOPT.

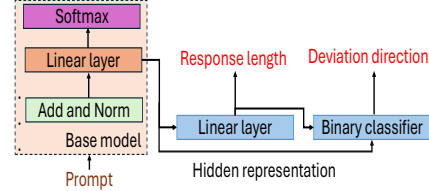


Figure 10: Our model for output length prediction.

and extend its architecture to predict response length, and deviation direction. As shown in Figure 10, we add two layers (in blue) after the last linear layer in the base model. This layer outputs the hidden representation of the input prompt, which is the input of our added linear layer. The added binary classifier outputs the deviation direction (0/1).

The added linear layer predicts the output length. The binary classifier is a fully connected layer. Its input includes the hidden representation of the last linear layer of the base model and that of our added linear layer.

The input to the model is the prompt itself. The fine-tuning is conducted in two steps. First, we fine-tune the model without the binary classifier using the ground-truth of the output lengths. Then, using the fine-tuned predictor, we predict the output lengths and collect the data of deviation direction. Second, we use this collected data to find-tune the whole model including the binary classifier.

Padding determination. For a given predicted output length, if its actual output lengths follow a specific probability distribution, the padding for the predicted output length can be determined based on this distribution to achieve a certain confidence. However, the probability distributions of the 9k fine-tuning requests and 6k inference requests does not follow a certain distribution. Therefore, this approach is not viable.

We then leverage the Hoeffding’s inequality theory. It is used to bound the deviation with a specified confidence. Let X_1, X_2, \dots, X_n be independent random variables, where $a_i \leq X_i \leq b_i$ for $i = 1, 2, \dots, n$. Let us define $S = X_1 + X_2 + \dots + X_n$ and use $E[S]$ to denote the expected value of the sum. Then, for any limit $t > 0$:

$$P(S - E[S] \geq t) \leq \exp\left(\frac{-2t^2}{\sum_{i=1}^n (b_i - a_i)^2}\right) \quad (1)$$

We use X_i as the actual output length of request i , \hat{X}_i as its

predicted length, t_i is the maximum allowed deviation, and $(b_i - a_i)$ defines the range of request length for request i in the predicted values. Then, Equation (1) becomes:

$$P((X_i - \hat{X}_i) \geq t_i) \leq \exp\left(\frac{-2t_i^2}{(b_i - a_i)^2}\right) \quad (2)$$

Let c_i be the specified confidence, i.e., $P((X_i - \hat{X}_i) \geq t_i) = 1 - c_i$. By solving the equation, we get:

$$t_i = \sqrt{-\frac{(b_i - a_i)^2}{2} \cdot \ln(1 - c_i)} \quad (3)$$

We use this t_i as the padding for underprediction. From Equation (3), higher c_i leads to more padding and vice versa. Padding t_i for overprediction is calculated similarly. Based on the deviation direction, the padding is added or subtracted from the predicted output length.

Based on O2, a higher request arrival rate results in longer waiting times, necessitating a lower padding size hence lower confidence, and vice versa. Thus, we propose dynamically adjusting c_i based on the request arrival rate λ :

$$c_i = \frac{\alpha}{1 + \beta\lambda}, \quad (4)$$

where $0 < \alpha \leq 1$ controls the maximum possible confidence, and $\beta > 0$ regulates the sensitivity of the confidence to the arrival rate changes. At low arrival rates ($\lambda \rightarrow 0$), the denominator $1 + \beta\lambda$ approaches 1, resulting in $c_i \approx \alpha$. As the arrival rate λ increases, the denominator grows, causing c_i to decrease. This reflects reduced confidence in predictions when KVC is limited for the requests. The parameters here are empirically determined.

3.3 SLO-aware Batching and KVC Allocation

This component tackles the challenge outlined in O1 by incorporating (1) an embedding method to reuse allocated but unused KVC (3.3.1), (2) a request selection and KVC allocation strategy (3.3.2), and (3) preemption-avoidance mechanisms (3.3.3). Key notations are summarized in Table 2.

Table 2: Summary of notations.

Notation	Description
SLO_{tft}	TTFT SLO.
SLO_{tbt}	TBT SLO.
N_w	Waiting requests that must execute next to meet SLO_{tft}
N_r	Returned requests that used up allocated KVC but must execute next to meet SLO_{tbt}
N_w'	Selected waiting requests that contribute to exhausting the token budget
N_r'	Returned requests that used up allocated KVC but not needing immediate execution
T_I^{max}	Maximum iteration latency historically observed
s_i^p	Prompt length of request i
s_i^o	Estimated output length of request i
M_i	Total KVC demand for request i : $M_i = s_i^p + s_i^o$
A_{kvc}^t	Unallocated KVC available for the current iteration
B	Fixed block size for KVC allocation
D_{kvc}	Total KVC demanded for critical requests: $D_{kvc} = \sum_i N_w (s_i^p + B) + \sum_r N_r B$
a_i	Allocated KVC for a running request i
u_i	Currently used/occupied KVC for a running request i
γ	Factor used to determine KVC allocation cuts based on SLO priority
E_{kvc}	Excess demanded KVC: $E_{kvc} = \sum M_i - A_{kvc}^t$

3.3.1 Embedding Method

As shown in Figure 11, a running request r_j 's allocated KVC is denoted by a_j and its currently used KVC is denoted by

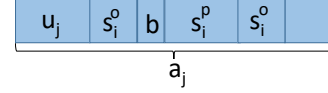


Figure 11: Embedding method to reuse allocated but unused KVC.

u_j . If another request r_i uses r_j 's allocated but unused KVC starting from the location marked by the red line, when both r_i and r_j run s_i^o iterations, r_i completes and releases its KVC and r_j has reached the point b tokens before r_i 's KVC space. b functions as a buffer to handle the inaccurate estimation and it is set to a small number (e.g., 8 tokens). Therefore, if $a_j - (u_j + s_i^o) - (s_i^p + s_i^o) \geq b$, it means that we can allocate r_i in the allocated KVC of r_j starting from the red line $s_0 = a_j - (u_j + s_i^o) - b$. To choose a request to embed request r_i , we choose the running request r_j that has the minimum remaining allocated KVC in order to reduce reserved waste. Due to inaccurate estimation of s_i^o , if r_i does not complete by the time when r_j needs the KVC allocated to r_i , then r_i must be preempted. The value of b is empirically determined; a larger b leads to higher reserved waste while a smaller b may cause the preemption of r_i .

3.3.2 Request Selection and KVC Allocation

The requests in a returned batch after an iteration are called *returned requests*. In forming a new batch and allocating KVC, we make sure that (1) the waiting requests' SLO_{tft} and the returned requests' SLO_{tbt} must be satisfied, and (2) we allocate the KVC to a request as close to its demand as possible to avoid preemptions to reduce TBTs while reducing reserved waste to reduce both TTFTs.

The waiting requests are ordered by the ascending order of their Remaining Time (RT) to their SLO_{tft} and the SLO_{tbt} for preempted requests, denoted by RT_{tft} and RT_{tbt} . The requests are sequentially selected to add to the batch. We use T_I^{max} to denote the maximum iteration latency historically. Then, the waiting requests that have $(RT_{tft} - T_I^{max}) < \epsilon$, where ϵ is a small number, must be batched in order to satisfy their SLO_{tft} . We use N_w to denote the group of such waiting requests, and N_r the group of returned requests that have used up their allocated KVC and must execute in the next iteration to satisfy their SLO_{tbt} , that is, $RT_{tbt} - T_I^{max} < \epsilon$. The requests in N_w and N_r are called *critical requests*, which need to allocate KVC first. Below, we present how to allocate KVC to critical requests and then to other returned requests and requests selected to exhaust the token budget (named as non-critical requests).

(1) Allocate KVC to critical requests. We define a small block (e.g., 8 blocks), denoted by B . The basic KVC requirement of a critical waiting request equals to the sum of its prompt length and a block size: $(s_i^p + B)$, and that of a critical returned request equals to B . The total basic KVC requirement

of critical requests equals to $D_{kvc} = \sum_i^{|\mathbf{N}_w|} (s_i^p + B) + \sum_i |\mathbf{N}_r| B$. We sort the critical requests in descending order of their basic requirements and allocate each request using the embedding method first. Then, we allocate the remaining critical requests to unallocated KVC. If the current unallocated KVC $A'_{kvc} < D_{kvc}$, preemptions are executed to make $A'_{kvc} = D_{kvc}$. Which requests to choose for preemptions is introduced in 3.4. When $A'_{kvc} \geq D_{kvc}$, we allocate the basic required KVC to each remaining critical request. Then, if there remains unallocated KVC, we allocate it to all critical requests and other non-critical requests. The details are presented below.

(2) Allocating remaining KVC for the next iteration.

We use \mathbf{N}'_r to denote the group of returned requests that are not critical. In addition to critical requests, \mathbf{N}'_r , we sequentially select requests from the waiting requests to use up the token budget (denoted by \mathbf{N}'_w) to minimize waiting time and maximize throughput. All non-critical requests (\mathbf{N}'_w and \mathbf{N}'_r) and critical requests (\mathbf{N}_w and \mathbf{N}_r) will join the KVC allocation. We use n to denote the total number of these requests. The next question is how to distribute A'_{kvc} among these requests. In this step, we allocate KVC to each request to match its total demand ($M_i = S_i^p + S_i^o$) as closely as possible while accommodating the n requests to the batch.

For non-critical requests, we use the embedding method first. If it successfully allocates a request, the request's M_i becomes 0. Then, we allocate A'_{kvc} to the remaining requests for the following three cases:

- When $\sum_{i=1}^n M_i = A'_{kvc}$, the requests are added to the batch and are guaranteed to receive the KVC they demand during execution.
- When $\sum_{i=1}^n M_i < A'_{kvc}$, adding more requests can more fully allocate the KVC, increase dequeuing speed and increase throughput slightly, but may also increase iteration time. The iteration time, estimated based on profiled data, increases almost linearly with the number of tokens in a batch [15]. Therefore, more requests are sequentially added from the queue until $\sum_{i=1}^n M_i = A'_{kvc}$ or the SLO of any request in the batch is violated.
- When $\sum_{i=1}^n M_i > A'_{kvc}$, we amortize the excess demands among the requests, and allow a request to use the released KVC from another request once the latter exhausts its allocated KVC. A request with a looser SLO and with a longer predicted output length should have a higher KVC demand cut since it is less delay-sensitive and also have more opportunities to receive KVC. Therefore, we incorporate these two factors in the amortization process. The weight for each request is computed as: $w_i = \frac{RT_i}{\sum_i RT_i} \times \frac{s_i^p}{\sum_i s_i^p}$. Subsequently, the KVC allocated to each request is determined by: $A_i = A'_{kvc} \times \frac{w_i}{\sum_{i=1}^n w_i}$. After the above amortization, a request r_i may not receive its demanded KVC fully. To address this, we find a running request r_j that will release its KVC shortly before r_i exhausts its allocated KVC, and the released KVC is no less than r_i 's additional demand. Then, r_i will use r_j 's released KVC.

3.3.3 Proactive KVC Allocation and Global Reservation

A request may not receive its KVC demand M_i (an unfulfilled request) and then if it exhausts its allocated KVC without any request completing, a preemption occurs. The proposed proactive KVC allocation and global reservation aim to avoid the preemptions. In the previous systems, completed requests' released KVC is used to accommodate requests from the waiting queue. To avoid preemptions, after allocating the KVC to the critical requests, we include unfulfilled running requests, predicted to complete within m iterations (where m is a small number), into the non-critical request group for the remaining KVC allocation.

Due to the autoregressive nature of LLMs and the imprecision in output length estimation, a request may not receive the necessary KVC when needed. Assigning additional padding to each request can lead to wasted reserved memory that may go unused. To address this, we reserve a shared KVC space for all requests, allowing them to use the space in case of KVC allocation failure.

3.4 Preemption Policy

The preemption policy determines the order for requests to be preempted to reduce both the number and duration of preemptions. Based on O3, CACHEOPT considers three factors: 1) TBT SLO, 2) SRTF, and 3) LKVO. The TBT SLO of a request needs to be satisfied so we choose a loose-SLO request to be preempted. The reasons for considering SRTF and LKVO are explained in 2.4. The remaining processing time is measured by the remaining predicted output tokens. For each factor, we set up certain magnitude ranges and order requests accordingly. For example, 0.05-0.2s, 0.2-0.5s, and 0.5-2s for the TBT SLO, and 0-128, 128-256, 256-384, 384-512, ... in tokens for the remaining processing time and occupied KV-cache. The requests first are ordered based on the descending order of TBT SLOs. Then, for the requests with similar TBT SLOs, they are ordered in the descending order of remaining processing time. Next, for the requests with similar remaining processing time, they are ordered in the ascending order of the KVC occupancy. Finally, CACHEOPT preempts the first request.

3.5 Preemption Strategy Selection

As per O4, if the sequence length is greater than a sweet spot, swapping is more time-efficient than recomputation. The key is to find this sweet spot. For this purpose, we can profiling and regression models for estimation.

Profiling is conducted using the LLM system with the specific settings including the type of GPUs, the number of GPUs, the tensor parallelism (TP) and model parallelism (MP) degrees and the model. For a given sequence length S , total memory bandwidth M_b and total GPU capacity G , of the target hardware (e.g., A100), we measure the recomputation

time for a range of sequence lengths, and use the data to train a polynomial regressor:

$$L_r(S) = \alpha_r \cdot S^{\beta_r} + \kappa_r \cdot S + \epsilon_r,$$

where α_r , β_r , κ_r and ϵ_r are parameters determined during training. We choose the polynomial regressor because recomputation latency typically involves complex operations like matrix multiplications and other non-linear computations that grow in polynomial complexity with the size of the input [16].

Similarly, we profile swapping times across various sequence lengths and use the results to train a linear regressor.:

$$L_s(S, M_b, G) = \gamma_s \cdot S + \delta_s,$$

where γ_s and δ_s are determined during training. We choose the linear regressor because swapping latency linearly increases based on the data size [17]. We calculate the sweet spot S_s , defined as the sequence length satisfying $L_r(S) = L_s(S)$.

4 Implementation

We implemented CACHEOPT based on the vLLM source code [6], comprising about 6K lines of Python code. To integrate confidence-based padding, we modified the *scheduler.py* file. Specifically, we added a new function, *compute_confidence_padding* and extended the *allocate_kv* function in vLLM to incorporate this padding method.

We modified *kvcache.py* to include our *embedding method*. We added a function named *form_batch* in the *scheduler.py*. We further added functionalities in the *allocate_kv* function to allocate KVC. New function *reuse_unused_kv* was integrated into the *TokenBlockManager* class in vLLM to reallocate unused KVC. We also added function *proactive_allocation* in *scheduler.py* to proactively allocate KVC.

We added another function *global_reservation* that sets up a reserved portion of the KVC. To track reserved KVC, in the *TokenBlockManager* class in *kvcache.py*, we added a function named *track_reserved_blocks* to manage the tracking, allocation, and release of reserved blocks. This function also ensures that the reserved blocks are separate from the general allocation pool, preventing conflicts during allocation. Function *allocate_reserved_kv* is added in *scheduler.py* to assign reserved KV-cache blocks to requests.

We replaced the default FCFS preemption policy in the *evict_request* function in vLLM with our preemption policy. Besides, we added a function, *preempt_request_strategy*, which decides the preemption strategy.

5 Performance Evaluation

Experiment Settings. Unless otherwise specified, the experiment settings are the same as in 2. For setting the TTFT and TBT SLO, we measured the average TTFT and TBT across all compared methods and multiply them by a SLO scale. The SLO scale was randomly selected from [0.5, 2.5]. Furthermore, to make the TTFT SLO reasonable for a long

prompt that needs chunking [18], we increased its TTFT SLO by multiplying it with a scaling factor equal to the number of chunks. We used 3-hour trace for OPT-13B and used 1-hour trace for OPT-175B. By default, we set the block size (B) to 8 tokens, the number of preallocation iterations m to 2, the number of reserved blocks to 8, the confidence to 90%, $\alpha = 8$, and $\beta = 100$, respectively.

Output length predictor. We used 9K requests and 6k for inference for testing the performance. The fine-tuning process took around 9 hours.

Compared Methods. We compared CACHEOPT with vLLM, RLP, S^3 , Sarathi-Serve (Sarathi for simplicity). Due to space limit, unless otherwise specified, we plot the average of the results across three datasets for each model.

5.1 Overall Performance Comparison

TTFT and TBT. Figures 12a, and 13a illustrate the *tail TTFT* during the entire running time versus the mean request arrival rate for different models. Figures 12b, and 13b, show the *TTFT SLO attainment*, which indicates the fraction of requests that meet their TTFT SLOs. We observe that the tail TTFT keeps increasing and the TTFT SLO attainment keep decreasing as the arrival rate increases. While the compared methods exhibit abrupt changes, CACHEOPT demonstrates a steady progression. CACHEOPT reduces the tail TTFT of vLLM, RLP, S^3 , and Sarathi by $64\%-2.34\times$, $1.21\times-2.83\times$, $1.11\times-2.73\times$, and $97\%-2.56\times$ across all arrival rates and models, respectively. Following a similar TTFT trend, CACHEOPT achieves 0.94-0.97 TTFT SLO attainment, with the highest improvement of 47% over Sarathi, the best compared system, at 40 req/s. This improvement stems from advanced methods that mitigate KVC bottlenecks to enable more requests per batch while reducing both the number and duration of preemptions, ultimately decreasing waiting time. The *confidence-based padding* method reduces preemptions, while the *embedding method* mitigate the KVC bottleneck. *Request selection and KVC allocation* tries to limit the TTFT. *Proactive KVC allocation* and *global KVC reservation* further reduce the preemptions. Additionally, CACHEOPT’s advanced preemption policy reduces the number and duration of preemptions. Further, *preemption strategy selection* minimizes swapping or recomputation time, allowing waiting requests to be scheduled earlier and reducing TTFT. Overall, the improvement for large models is smaller compared to small models due to reduced KVC competition when using more GPUs.

Figures 12c, and 13c illustrate the *tail TBT* during the entire experiment. Figures 12d, and 13d show the *TBT SLO attainment*, which indicates the fraction of requests whose all iterations meet their TBT SLOs. Similarly, as the arrival rate increases, while the compared methods exhibit abrupt changes, CACHEOPT demonstrates a steady progression. CACHEOPT achieves the lowest tail TBT among all systems. Specifically, CACHEOPT reduces the tail TBT of

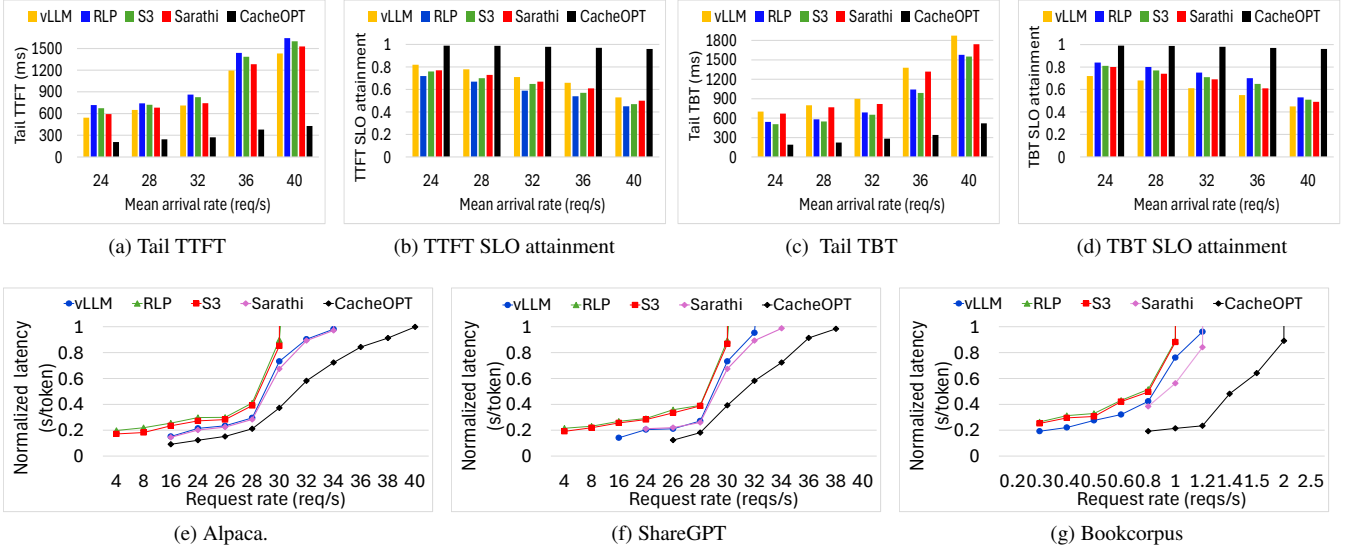


Figure 12: End-to-end latency performance for OPT-13B.

vLLM, RLP, S^3 , and Sarathi by $1.82\text{-}3.29\times$, $1.42\text{-}2.37\times$, $1.31\text{-}2.30\times$, and $1.47\text{-}2.71\times$ across all arrival rates and models. CACHEOPT achieves 0.94-0.98 TBT SLO attainment, outperforming Sarathi by 53% at 40 req/s. The superior performance of CACHEOPT can be attributed to its advanced strategies explained above. Mitigating KVC competition also reduces preemptions. The reduction of the number and duration of preemptions directly reduces TBT and avoid TBT SLO violations. Considering TBT SLO in selecting requests in batching and for preemptions further reduce TBT and avoid TBT SLO violations.

Normalized latency. *Normalized latency* is a request’s end-to-end latency divided by its output length [4, 6]. Figures 12e-12g, and 13e-13g show the average normalized latency of the systems versus the mean arrival rate. A high-throughput serving system should retain low normalized latency against high request rates. We compare the request rates that the systems can sustain while maintaining similar latencies. CACHEOPT can sustain $1.29\text{-}1.89\times$ higher arrival rates than vLLM, $1.44\text{-}1.94\times$ than RLP and S^3 , and $1.24\text{-}1.58\times$ than Sarathi on average for the three datasets. CACHEOPT’s advantages on BookCorpus is more pronounced because it contains longer sequences, allowing fewer requests to be batched and generating more KVC competition.

Similar to the tail TTFT, for other metrics, CACHEOPT shows lower improvement for larger models compared to smaller models and as arrival rates increase, CACHEOPT demonstrates greater improvements over other systems due to the same reasons.

5.2 Ablation Study

We tested the following variants of CACHEOPT to evaluate the effectiveness of its components.

- /CKA: CACHEOPT without Confident-based KVC Allocation and it adds a fixed padding of 10% of the predicted output length.
- /RSA: CACHEOPT without Result Selection and KVC Allocation and it uses FCFS for request selection and allocates KVC using RLP.
- /PA: CACHEOPT without Proactive KVC allocation.
- /GR: CACHEOPT without Global Reservation
- /PP: CACHEOPT without Preemption Policy and it follows FCFS.
- /PSS: CACHEOPT without Preemption Strategy Selection and it uses the default recomputation in the vLLM code.

Figures 14, and 15 show the different metrics of the variants in the four models. We now discuss the average results across the four models. CACHEOPT reduces the tail TTFT by 35%, 44%, 29%, 24%, 27%, 28% compared to /CKA, /RSA, /PA, /GR, /PP, and /PSS, respectively. For TTFT SLO attainment, these variants exhibit degradation of 27%, 34%, 26%, 23%, 14%, and 17%, respectively. For TBT, CACHEOPT demonstrates improvements of 40%, 48%, 35%, 29%, 25% and 27% compared to these variants, respectively. TBT SLO attainment for these variants shows degradations of 22%, 28%, 21%, 20%, 8%, and 13%, respectively. This demonstrates that removing or replacing critical design elements leads to performance degradation, and the critical role of all design components in reducing tail TTFT and TBT, and SLO violations.

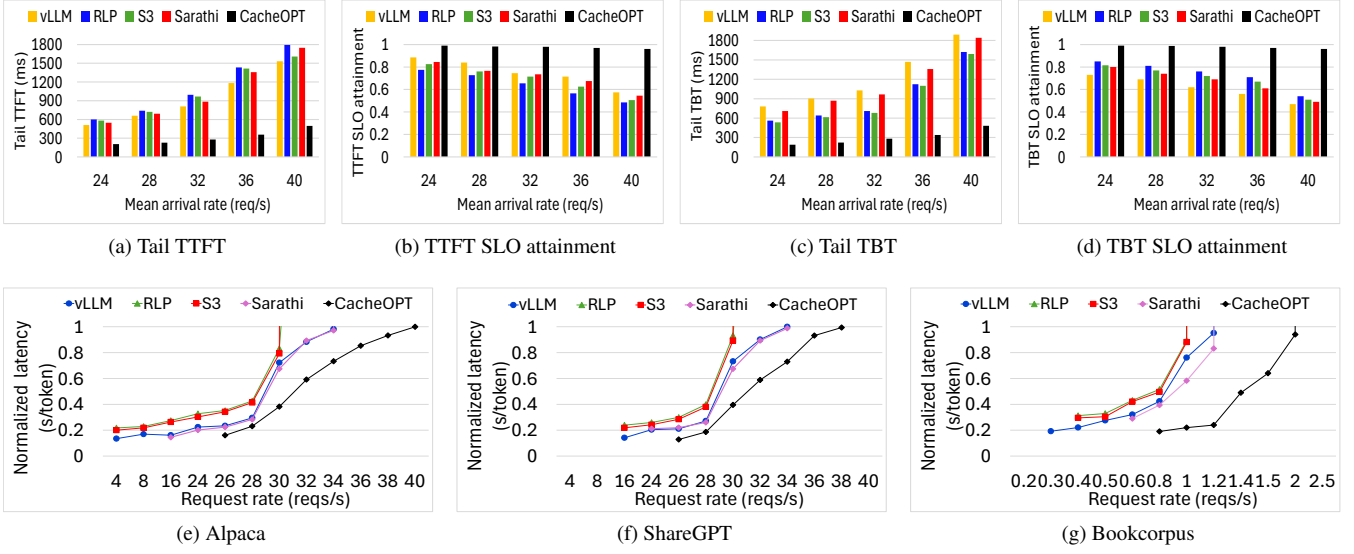


Figure 13: End-to-end latency performance for OPT-175B.

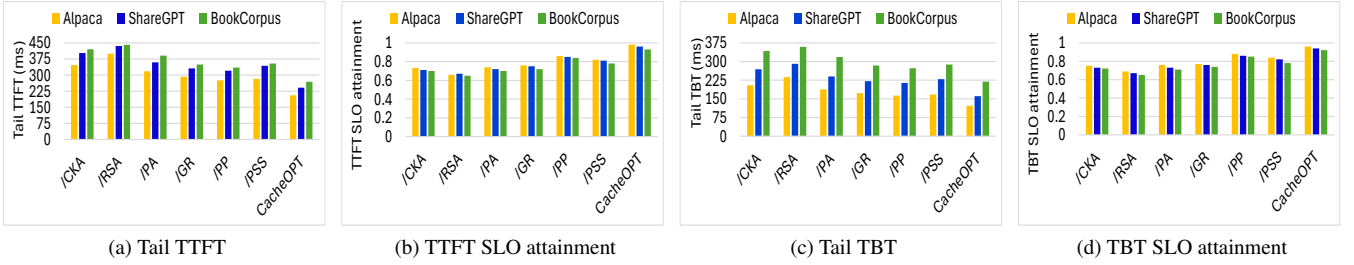


Figure 14: Ablation study for OPT-13B.

5.3 Time Overhead

Figure 16 shows the time overhead for different systems and for different variants of CACHEOPT in each iteration. CACHEOPT have 80%, 77%, 18%, and 23% higher time overhead than vLLM, Sarathi, RLP and S^3 respectively. These higher time overheads only constitute 0.003% over the iteration. The overhead of the components of the CACHEOPT contributes to its time overhead. Specifically, compared to the CACHEOPT, /CKA, /RSA, /PA, /GR, /PP, /PPS show 17%, 41%, 3%, 3.14%, 7%, 1.8% less time overhead, indicating the time overhead of each component.

5.4 Sensitivity Testing

Figure 17a shows the SLO attainment for the two OPT models, versus the SLO scale. The figure show a steady increase in SLO attainment as the scale increases. At the smallest scale of 0.5, CACHEOPT still can achieve around 0.85 TTFT and TBT SLO attainments. As the scale increases to 1.5, the SLO attainments surpass 0.95, and they reach nearly 1.0 at the

scale of 2.5. The results verify the capability of CACHEOPT in providing high TTFT and TBT SLO attainments, and good user experience.

Figures 17b shows the SLO attainments versus the block size (B). As the block size increases from 4 to 8, the SLO attainment increases, then as the block size increases, the SLO attainments gradually decrease. A smaller block size (e.g., 4) results in underprovisioning, which also leads to high TBT and hence high TTFT, though they do not increase significantly. This is because requests with insufficient KVC can still obtain additional KVC proactively or on demand. Conversely, a larger block size causes overprovisioning, reducing the number of requests per batch and increasing TTFT and KVC competition and hence TBT. Experimental results indicate that a block size of 8 performs best in our setup.

Figure 17c shows the SLO attainments versus the number of iterations for preallocation (m). At $m = 1$, SLO attainments are around 0.85, peaking at 1.0 when $m = 2$, before gradually declining beyond $m = 2$ due to reserved waste. Hence, $m = 2$ is the optimal setting in our experimental setup.

Figure 17d shows the SLO attainments versus the number

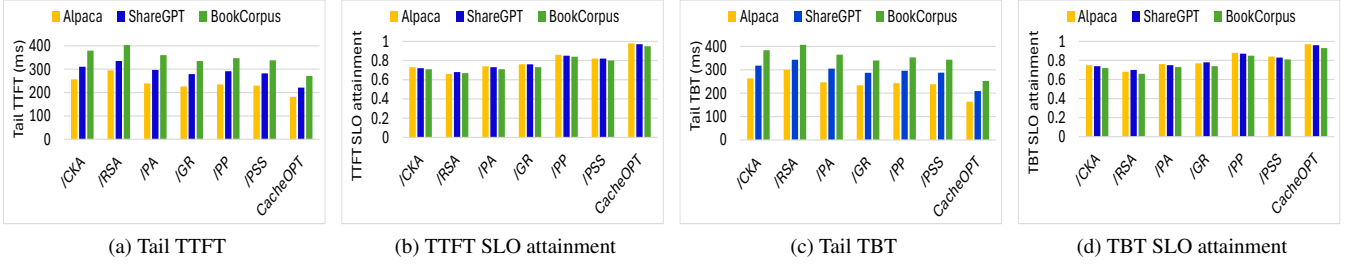


Figure 15: Ablation study for OPT-175B.

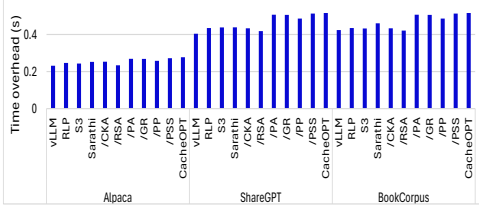


Figure 16: Scheduling time overhead.

of reserved blocks. The SLO attainments increase as the number of reserved blocks increases from 2 to 4 and then to 8, but then decrease when it keeps decreasing. Insufficient reserved KVC cannot satisfy KVC demands from some requests but high reservation increases reserved waste. Therefore, 4 and 8 are suitable number of reserved blocks in our experiment settings.

Figure 17e shows the impact of the variable α in Equation (4), which controls the Hoeffding’s inequality for CACHEOPT with β . For $\beta = 100$, with the increase of α , we observe that the TTFT SLO keeps increasing, but the TBT SLO keeps decreasing. This happens because increasing α increases c_i , which increases padding. Figure 17f shows the same plot for β , for $\alpha = 0.9$. For increasing β , we observe that TTFT SLO keeps decreasing while the TBT SLO keeps increasing, because increasing β decreases c_i , which decreases padding.

Figure 17g shows the impact of confidence score. The results demonstrate a trend of increasing TBT SLO attainments and decreasing TTFT SLO attainments as the confidence score increases. At lower confidence score (e.g., 80%), less padding is added, enabling more requests accommodated in a batch, which reduces waiting time but increases preemption time. At a confidence score of 0.9, both TTFT and TBT SLO attainments exceed 0.9, striking a balance between TTFT and TBT.

Figure 17h shows the impact of the confidence score on the number of overprovisions and underprovisions, along with their deviations. We also include those of RLP and S³ as reference. From the figure, we observe compared to RLP and S³ CACHEOPT’s response length predictor have 54% and

29% fewer overpredictions and 72% and 57% of lower underpredictions, respectively. We also see for overprediction, CACHEOPT’s response length predictor show 72% and 65% less deviation and 57% and 65% less deviation for underprediction, compared to RLP and S³, respectively. With the increase of the confidence score, more padding is added following Hoeffding’s inequality. As a result, fewer overprediction and underprediction requests are observed as it increases both positive and negative padding. We also observe the same phenomenon on the average deviation.

Overall, these results demonstrate the adaptability of CACHEOPT across a wide range of configurations. By effectively adapting KV cache allocation with workload demands, CACHEOPT maintains high SLO attainments, ensuring reliable performance under diverse conditions.

6 Limitations and Discussions

Model Assumptions: The effectiveness of Hoeffding’s inequality relies on the assumptions of bounded and independent random variables. While request lengths are naturally bounded, the independence assumption might not hold perfectly in real-world LLM service scenarios due to potential correlations between requests or workload patterns.

Confidence Score Calibration: CACHEOPT heavily depends on the accuracy and calibration of the confidence scores associated with predicted request lengths. If the confidence scores are not well-calibrated (i.e., they don’t accurately reflect the actual probabilities), the probabilistic guarantees offered by Hoeffding’s inequality might not hold in practice.

7 Related Work

ORCA [4] uses an iteration-level scheduling strategy combined with maximum resource allocation, which results in under-utilization of GPU resources. To address this inefficiency, vLLM [6] introduces a block-based allocation strategy, and prediction-based KVC allocation methods [5, 7] predict output lengths and allocate the KVC equal to the predicted size. Sarathi-Serve [19] incorporates chunked-prefills

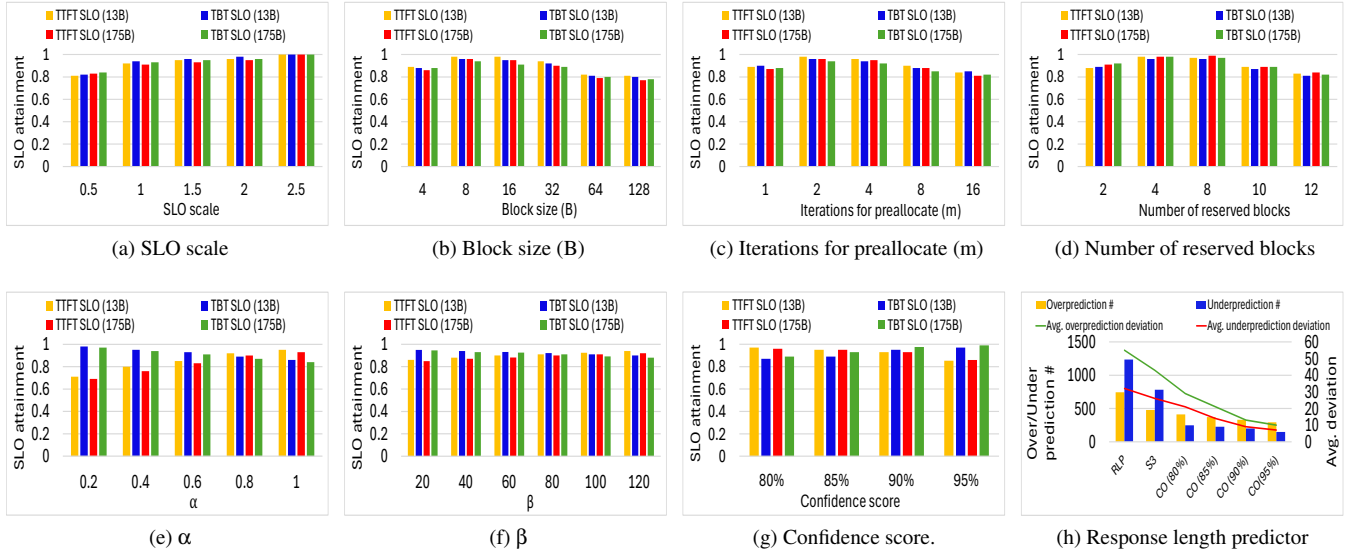


Figure 17: Sensitivity testing.

and stall-free scheduling to address long sequences. FastServe [20] utilizes preemptive scheduling to minimize JCT. Llumnix [2] reschedules requests across multiple model instances, effectively reducing tail latencies. vAttention [21] is a memory management system that uses virtual memory to store and manage the KV cache. Cheng *et al.* [22] developed a scheduling method that splits long-generation tasks into smaller parts, to make it easier to manage resources and predict serving times. ALISA [23] combines a Sparse Window Attention algorithm to reduce the memory footprint of KVC with three-phase token-level dynamic scheduling to optimize the balance between caching and recomputation. Several approaches focus on resource optimization to improve LLM performance. ExeGPT [24] optimizes resource usage and adjusts execution settings like batch size and parallelism. INFERMAX [25] analyzes different scheduling strategies, focusing on balancing costs and resource usage. Sheng *et al.* [26] focused on achieving fairness in scheduling. Lee *et al.* [27] proposed prefetching only the essential KV cache entries for computing the subsequent attention layer. DistServe [28] decouples the prefill and decode phases, running them on separate machines or GPUs. Some other methods [29, 30] aim to enhance the efficiency and performance of LLM applications either by optimizing application-level operations or by dynamic adapter management targeting LoRA. Unlike previous work, we study the impact of the allocated KVC amount on the tradeoff between satisfying the TTFT and TBT SLOs, and propose novel methods to maximize the attainment of both TTFT and TBT SLOs.

8 Conclusion

Our proposed CACHEOPT addresses the challenge to satisfy both TTFT and TBT SLOs. It incorporates four components: 1) confidence-based padding, 2) SLO-aware batching and KVC allocation, 3) preemption policy, and 4) preemption strategy selection. Experimental results show that CACHEOPT achieves up to a $3.29\times$ and $2.83\times$ lower tail TBT and TTFT, and 47% and 53% higher TTFT and TBT SLO attainment than the state-of-the-art methods. In the future, we will design methods to automatically determine the optimal parameters in CACHEOPT.

References

- [1] Seldon. Deploying large language models in production: Llm deployment challenges. <https://shorturl.at/sE8qZ>, 2023.
- [2] Biao Sun, Ziming Huang, Hanyu Zhao, Wencong Xiao, Xinyi Zhang, Yong Li, and Wei Lin. Llumnix: Dynamic scheduling for large language model serving. *Proc. of OSDI*, 2024.
- [3] Qianchao Zhu, Jiangfei Duan, Chang Chen, Siran Liu, Xiuhong Li, Guanyu Feng, Xin Lv, Huanqi Cao, Chuanfu Xiao, Xingcheng Zhang, Dahua Lin, and Chao Yang. Sampleattention: Near-lossless acceleration of long context llm inference with adaptive structured sparse attention. *ArXiv*, abs/2406.15486, 2024.
- [4] Gyeong-In Yu, Joo Seong Jeong, Geon-Woo Kim, Soo-jeong Kim, and Byung-Gon Chun. Orca: A distributed

- serving system for Transformer-Based generative models. In *16th USENIX Symposium on Operating Systems Design and Implementation (OSDI 22)*, 2022.
- [5] Yunho Jin, Chun-Feng Wu, David Brooks, and Gu-Yeon Wei. S³: Increasing gpu utilization during generative inference for higher throughput. *arXiv preprint arXiv:2306.06000*, 2023.
 - [6] Woosuk Kwon, Zhuohan Li, Siyuan Zhuang, Ying Sheng, Lianmin Zheng, Cody Hao Yu, Joseph E. Gonzalez, Haoteng Zhang, and Ion Stoica. Efficient memory management for large language model serving with pagedattention. *Proceedings of the 29th Symposium on Operating Systems Principles*, 2023.
 - [7] Zangwei Zheng, Xiaozhe Ren, Fuzhao Xue, Yang Luo, Xin Jiang, and Yang You. Response length perception and sequence scheduling: An LLM-empowered LLM inference pipeline. In *Thirty-seventh Conference on Neural Information Processing Systems*, 2023.
 - [8] Yunho Jin, Chun-Feng Wu, David M. Brooks, and Gu-Yeon Wei. S³: Increasing gpu utilization during generative inference for higher throughput. *ArXiv*, abs/2306.06000, 2023.
 - [9] Wassily Hoeffding. Probability inequalities for sums of bounded random variables. *Journal of the American Statistical Association*, 58(301):13–30, 1963.
 - [10] Vidmantas Bentkus. On hoeffding’s inequalities. *Annals of probability*, pages 1650–1673, 2004.
 - [11] Susan Zhang, Stephen Roller, Naman Goyal, Mikel Artetxe, Moya Chen, Shuohui Chen, Christopher Dewan, Mona T. Diab, Xian Li, Xi Victoria Lin, Todor Mihaylov, Myle Ott, Sam Shleifer, Kurt Shuster, Daniel Simig, Punit Singh Koura, Anjali Sridhar, Tianlu Wang, and Luke Zettlemoyer. Opt: Open pre-trained transformer language models. *ArXiv*, 2022.
 - [12] Rohan Taori, Ishaan Gulrajani, Tianyi Zhang, Yann Dubois, Xuechen Li, Carlos Guestrin, Percy Liang, and Tatsunori B. Hashimoto. Stanford alpaca: An instruction-following llama model. https://github.com/tatsu-lab/stanford_alpaca, 2023.
 - [13] ShareGPT. sharegpt-english. <https://huggingface.co/datasets/theblackcat102/sharegpt-english>, 2023.
 - [14] Sosuke Kobayashi. Homemade bookcorpus. <https://github.com/soskek/bookcorpus>, 2018.
 - [15] Amey Agrawal, Ashish Panwar, Jayashree Mohan, Nipun Kwatra, Bhargav S. Gulavani, and Ramachandran Ramjee. Stablegen: Efficient llm inference with low tail latency. *Proc. of OSDI*, 2024.
 - [16] Deepak Narayanan, Mohammad Shoeybi, Jared Casper, Patrick LeGresley, Mostofa Patwary, Vijay Korthikanti, Dmitri Vainbrand, Prethvi Kashinkunti, Julie Bernauer, Bryan Catanzaro, et al. Efficient large-scale language model training on gpu clusters using megatron-lm. In *Proceedings of the International Conference for High Performance Computing, Networking, Storage and Analysis*, pages 1–15, 2021.
 - [17] Nvidia. Megatron-LM. <https://github.com/NVIDIA/Megatron-LM>. Online; accessed in April 2024.
 - [18] Microsoft. DeepSpeed-FastGen: High-throughput Text Generation for LLMs via MII and DeepSpeed-Inference. <https://github.com/microsoft/DeepSpeed/tree/master/blogs/deepspeed-fastgen>. Online; accessed in April 2024.
 - [19] Amey Agrawal, Nitin Kedia, Ashish Panwar, Jayashree Mohan, Nipun Kwatra, Bhargav Gulavani, Alexey Tumanov, and Ramachandran Ramjee. Taming {Throughput-Latency} tradeoff in {LLM} inference with {Sarathi-Serve}. In *18th USENIX Symposium on Operating Systems Design and Implementation (OSDI 24)*, pages 117–134, 2024.
 - [20] Bingyang Wu, Yinmin Zhong, Zili Zhang, Gang Huang, Xuanzhe Liu, and Xin Jin. Fast distributed inference serving for large language models. *ArXiv*, abs/2305.05920, 2023.
 - [21] Ramya Prabhu, Ajay Nayak, Jayashree Mohan, Ramachandran Ramjee, and Ashish Panwar. vattention: Dynamic memory management for serving llms without pagedattention. *ArXiv*, abs/2405.04437, 2024.
 - [22] Ke Cheng, Wen Hu, Zhi Wang, Hongen Peng, Jianguo Li, and Sheng Zhang. Slice-level scheduling for high throughput and load balanced llm serving. *ArXiv*, abs/2406.13511, 2024.
 - [23] Youpeng Zhao, Di Wu, and Jun Wang. Alisa: Accelerating large language model inference via sparsity-aware kv caching. *2024 ACM/IEEE 51st Annual International Symposium on Computer Architecture (ISCA)*, pages 1005–1017, 2024.
 - [24] Hyungjun Oh, Kihong Kim, Jaemin Kim, Sungkyun Kim, Junyeol Lee, Du-seong Chang, and Jiwon Seo. Exegpt: Constraint-aware resource scheduling for llm inference. *CoRR*, abs/2404.07947, 2024. Accepted to ASPLOS 2024 (summer cycle).
 - [25] Kyoungmin Kim, Kijae Hong, Caglar Gulcehre, and Anastasia Ailamaki. The effect of scheduling and preemption on the efficiency of llm inference serving. *arXiv preprint arXiv:2411.07447*, 2024.

- [26] Ying Sheng, Shiyi Cao, Dacheng Li, Banghua Zhu, Zhuohan Li, Danyang Zhuo, Joseph E. Gonzalez, and Ion Stoica. Fairness in serving large language models. In *Proceedings of OSDI*, 2024.
- [27] Wonbeom Lee, Jungi Lee, Junghwan Seo, and Jaewoong Sim. InfiniGen: Efficient generative inference of large language models with dynamic KV cache management. In *18th USENIX Symposium on Operating Systems Design and Implementation (OSDI 24)*, pages 155–172, Santa Clara, CA, July 2024. USENIX Association.
- [28] Yinmin Zhong, Shengyu Liu, Junda Chen, Jianbo Hu, Yibo Zhu, Xuanzhe Liu, Xin Jin, and Hao Zhang. Dist-Serve: Disaggregating prefill and decoding for goodput-optimized large language model serving. In *18th USENIX Symposium on Operating Systems Design and Implementation (OSDI 24)*, pages 193–210, Santa Clara, CA, July 2024. USENIX Association.
- [29] Bingyang Wu, Ruidong Zhu, Zili Zhang, Peng Sun, Xuanzhe Liu, and Xin Jin. dLoRA: Dynamically orchestrating requests and adapters for LoRA LLM serving. In *18th USENIX Symposium on Operating Systems Design and Implementation (OSDI 24)*, pages 911–927, Santa Clara, CA, July 2024. USENIX Association.
- [30] Chaofan Lin, Zhenhua Han, Chengruidong Zhang, Yuqing Yang, Fan Yang, Chen Chen, and Lili Qiu. Parrot: Efficient serving of LLM-based applications with semantic variable. In *18th USENIX Symposium on Operating Systems Design and Implementation (OSDI 24)*, pages 929–945, Santa Clara, CA, July 2024. USENIX Association.